

Kinematics of globular cluster systems and the formation of early-type galaxies

K. Bekki,¹ Michael A. Beasley², Jean P. Brodie², and Duncan A. Forbes³

¹*School of Physics, University of New South Wales, Sydney, NSW 2052, Australia*

²*UCO/Lick Observatory, University of California, Santa Cruz, CA 95064*

³*Centre for Astrophysics and Supercomputing, Swinburne University of Technology, Hawthorn, VIC 3122, Australia*

Accepted Received in original form 2001

ABSTRACT

We numerically investigate the kinematic properties of globular cluster systems (GCSs) in E/S0 galaxies formed from dissipationless merging of spiral galaxies. The metal-poor globular clusters (MPCs) and metal-rich clusters (MRCs) in the merger progenitors are initially assumed to have spatial distributions consistent with the Milky Way GC system. Our principal results, which can be tested against observations, are as follows. Both MPCs and MRCs in elliptical galaxies formed from major mergers can exhibit significant rotation at large radii (~ 20 kpc) due to the conversion of initial orbital angular momentum into intrinsic angular momentum of the remnant. MPCs show higher central velocity dispersions than MRCs for most major merger models. V_m/σ_0 (where V_m and σ_0 are the GCS maximum rotational velocity and central velocity dispersion of respectively) ranges from 0.2–1.0 and 0.1–0.9 for the MPCs and MRCs respectively, within $6R_e$ for the remnant elliptical. For most merger remnant ellipticals, V_m/σ_0 of GCSs within $6R_e$ is greater than that of the field stars within $2R_e$. The radial profiles of rotational velocities and velocity dispersions of the GCSs depend upon the orbital configuration of the merger progenitors, their mass-ratios, and the viewing angle. For example, more flattened early-type galaxies, formed through mergers with small mass ratios (~ 0.1), show little rotation in the outer MRCs. Two-dimensional (2D) velocity dispersion distributions of the GCSs of merger remnant ellipticals are generally flattened for both MPCs and MRCs, reflecting the fact that the GCSs have anisotropic velocity dispersions. The 2D distributions of line-of-sight-velocity of the GCSs in some remnant ellipticals show minor-axis rotation, particularly for MRCs. The kinematic properties of MPCs in merger remnant ellipticals strongly resemble those of the surrounding dark matter. This implies that the kinematics of MPCs in such galaxies can be used to probe the kinematic properties of their dark matter halos. We discuss these results in the context of GC and galaxy formation. We note a possible difference in the GC kinematics between field and cluster Es and explain how GC kinematics may help us understand the origin of S0 galaxies.

Key words: globular clusters: general – galaxies: evolution – galaxies: elliptical and lenticular, cD – galaxies: kinematics and dynamics – galaxies: interaction

1 INTRODUCTION

The properties of globular cluster systems (GCSs) in galaxies have long been considered as fossil records of galaxy formation and subsequent evolutionary processes. These properties have been discussed in various different contexts of galaxy formation (Searle & Zinn 1978; Forbes et al. 1997; Ashman & Zepf 1998; Beasley et al. 2002; Brodie et al. 1998; Côte et al. 2000). The specific frequencies (S_N), colour bimodality, and structural properties of GCSs have received

particular attention, generally focusing on origin of early-type (E/S0) galaxies.

The kinematics of GCSs, however, has not been extensively studied. This is largely due to the practical difficulties of obtaining large kinematic samples of globular clusters (GCs). However, GC kinematics do offer important insights into galaxy halo properties and galaxy formation processes. GCs in a galaxy are observable test particles which trace the underlying gravitational potential beyond several effective radii (R_e), where the dark matter halo is thought to domi-

nate the mass density. Therefore, the kinematics of GCs allow an estimation of the global mass distribution of a galaxy, including the dark matter halo. In addition, kinematical differences between GCs with different chemical properties can provide constraints on the formation processes of the galaxy. This is analogous to the studies of stellar metallicities and kinematics (i.e., orbital eccentricities) in the Galactic halo used to assess the time scale of gravitational collapse of the Galaxy (e.g., Eggen, Lynden-Bell & Sandage 1962).

Until recently, the lack of highly-multiplexing spectrographs on large telescopes has meant that GC kinematics in only a handful of early-type galaxies have been studied in detail. They include M87 with 278 GC velocities (Côte et al. et al. 2001; Cohen & Ryzhov 1997; Mould et al. 1990), NGC 4472 with 263 (Côte et al. 2003; Zepf et al. 2000; Sharples et al. 1998; Mould et al. 1990), NGC 5128 with 215 GCs (Peng et al. 2004a; Sharples 1988; Hesser, Harris & Harris 1986) and NGC 1399 with 468 GCs (Richtler et al. 2004; Minniti et al. 1998; Grillmair et al. 1994). Because of this small galaxy sample, it is difficult to draw any general conclusions. For example, in M87 (Côte et al. 2001) the red GCs rotate about the galaxy minor axis, and the velocity dispersion is roughly constant with radius ($\langle \sigma \rangle \sim 397$ km/s). The outer blue GCs also rotate about the minor axis, but the inner ones rotate about the major axis. The velocity dispersion increases slightly with radius ($\langle \sigma \rangle \sim 364$ km/s). In NGC 4472 (Côte et al. 2003), the red GCs do not rotate and the velocity dispersion is constant with radius ($\langle \sigma \rangle \sim 265$ km/s). The blue GCs rotate about the minor axis, and also have a near constant velocity dispersion ($\langle \sigma \rangle \sim 342$ km/s).

Various numerical simulations on the formation of GCs in galaxies have been used to better understand the observed properties of GCs (e.g., Weil & Pudritz 2001; Bekki et al. 2002; Bekki & Chiba 2002; Kravtsov & Gnedin 2003; Li et al. 2004). However, much of this work has focused on the origin of specific frequency (S_N) of GCs in ellipticals, GC metallicity distributions, and color bimodality, rather than on GC kinematical properties. Thus, at present, there are few model predictions that can be compared with the above observations. The latest observations of extragalactic GCSs, based on multi-object spectrographs on large telescopes are providing unprecedentedly rich data on kinematical properties of the GCSs (e.g., Richtler et al. 2004).

Comparison between these kinematical data and numerical simulations not only allows investigation of the structure of dark matter halos (e.g., Peng et al. 2004a), but will also help us to understand the formation processes of galaxies themselves.

The purpose of this paper is to provide some observable predictions of the kinematics of GCSs in early-type galaxies based upon dissipationless numerical simulations of galaxy mergers. We adopt a reasonable set of parameters for the initial structural and kinematical properties of GCSs in the merger progenitor spirals, and thereby investigate dynamical evolution of the GCSs during galaxy merging. The initial GCSs in merger progenitor spirals are assumed to be composed of old metal-poor GCs (MPCs) and old metal-rich clusters (MRCs), that are associated with their halos and bulges/thick disks respectively. We investigate the structural and kinematical properties of these MPCs and MRCs, but do not address the properties of young, metal-rich GCS that

may be formed during galaxy mergers with gas (Bekki et al. 2002). These objects are expected to have quite different characteristics due to gas dissipation (Bekki et al. 2002; Li et al. 2004), and appear to make up only a small fraction of the metal-rich peak of GCSs (e.g., Brodie et al. 2004). We investigate radial profiles of rotational velocities and velocity dispersions of GCSs in merger remnants (i.e., E/SOs) and their dependencies on the physical parameters of galaxy merging, such as the orbital configuration and the mass ratio of the merger progenitors.

The plan of the paper is as follows: In the next section, we describe our numerical models for dynamical evolution of GCs in dissipationless galaxy mergers. In §3, we present the numerical results on structural and kinematical properties of MPCs and MRCs in the merger remnants. In §4, we discuss the derived numerical results in several different contexts of galaxy formation and evolution, such as cluster and field E formation. We summarise our conclusions in §5.

2 THE MERGER MODEL

2.1 Progenitor spiral galaxies

Since the numerical methods and techniques we employ for modeling dynamical evolution of galaxy mergers have already been detailed elsewhere (Bekki & Shioya 1998), we give only a brief review here. The progenitor disk galaxies that take part in a merger are given a dark halo, a bulge, a stellar halo, a thin exponential disk, MPCs, and MRCs. The total disk mass and size are M_d and R_d , respectively. Henceforth, all masses are measured in units of M_d and distances in units of R_d , unless otherwise specified. Velocity and time are measured in units of $v = (GM_d/R_d)^{1/2}$ and $t_{\text{dyn}} = (R_d^3/GM_d)^{1/2}$, respectively, where G is the gravitational constant and assumed to be 1.0 in the present study. If we adopt $M_d = 6.0 \times 10^{10} M_\odot$ and $R_d = 17.5$ kpc as fiducial values, then $v = 1.21 \times 10^2$ km s $^{-1}$ and $t_{\text{dyn}} = 1.41 \times 10^8$ yr.

We adopt the density distribution of the NFW halo (Navarro, Frenk & White 1996) suggested from CDM simulations:

$$\rho(r) = \frac{\rho_0}{(r/r_s)(1+r/r_s)^2}, \quad (1)$$

where r , ρ_0 , and r_s are the spherical radius, the central density of a dark halo, and the scale length of the halo, respectively. The dark matter to disk mass ratio is fixed at 9 for all models. The value of r_s (typically $\sim 3R_d$) is chosen such that the rotation curve of the disk is reasonably consistent with observations for a given bulge mass. The $R^{1/4}$ bulge has a mass of 0.17 and a scale length of 0.04, both of which are consistent with observations for the Galactic bulge (e.g., van den Bergh 2000).

The radial (R) and vertical (Z) density profiles of the disk are assumed to be proportional to $\exp(-R/R_0)$ with scale length $R_0 = 0.2$ and to $\text{sech}^2(Z/Z_0)$ with scale length $Z_0 = 0.04$ in our units, respectively. In addition to the rotational velocity attributable to the gravitational field of the disk and halo components, the initial radial and azimuthal velocity dispersions are added to the disk component in accordance with the epicyclic theory, and with a Toomre parameter value of $Q = 1.5$ (Binney & Tremaine 1987). The

Table 1. Model parameters

Model no. ^a	m_2	e_p	r_p ^b	θ_1	θ_2	ϕ_1	ϕ_2	$a_{\text{mrc}}/a_{\text{mpc}}^c$	t_v^d	R_e^e	$R_{e,\text{mpc}}^f$	$R_{e,\text{mrc}}^g$	Comments
PM1	1.0	1.0	1.0	30	60	90	0	0.5	–	0.37	0.96	0.53	fiducial
PM2	1.0	1.0	1.0	0	30	0	0	0.5	–	0.39	0.98	0.50	prograde-prograde
PM3	1.0	1.0	1.0	150	180	0	0	0.5	–	0.36	0.93	0.50	retrograde-retrograde
PM4	1.0	1.0	0.2	30	60	90	0	0.5	–	0.39	1.00	0.53	smaller angular momentum
PM5	1.0	0.7	1.0	30	60	90	0	0.5	–	0.33	0.85	0.47	elliptic orbit
PM6	1.0	1.0	1.0	0	150	90	0	0.5	–	0.37	0.93	0.51	prograde-retrograde
PM7	0.1	1.0	0.5	0	30	0	0	0.5	–	0.31	0.62	0.34	
PM8	0.3	1.0	0.5	0	30	0	0	0.5	–	0.36	0.81	0.42	
PM9	1.0	1.0	0.5	0	30	0	0	0.5	–	0.49	1.15	0.59	
PM10	0.1	1.0	0.5	0	30	0	0	0.1	–	0.32	0.63	0.10	
PM11	0.3	1.0	0.5	0	30	0	0	0.1	–	0.37	0.90	0.17	
PM12	1.0	1.0	0.5	0	30	0	0	0.1	–	0.50	1.09	0.13	
MM1	1.0	–	–	–	–	–	–	0.5	0.50	0.77	1.31	0.95	dispersion supported ^h
MM2	1.0	–	–	–	–	–	–	0.5	0.75	0.75	1.45	0.98	dispersion supported
MM3	1.0	–	–	–	–	–	–	0.5	0.25	0.73	1.21	0.87	dispersion supported
MM4	1.0	–	–	–	–	–	–	0.5	0.50	0.64	1.08	0.75	rotation supported ⁱ
MM5	1.0	–	–	–	–	–	–	0.5	0.75	0.69	1.17	0.79	rotation supported
MM6	1.0	–	–	–	–	–	–	0.5	0.25	0.61	1.01	0.73	rotation supported

^a PM and MM describe pair merger and multiple mergers, respectively.

^b Pericenter distance in units of R_d ($=17.5$ kpc)

^c Scale length ratio of MRCs to MPCs.

^d The ratio of initial kinematic (either rotational or random) energy to potential energy in a multiple merger.

^e The half-mass radius of stars in simulation units of R_d ($=17.5$ kpc). The real scale of the effective radius of an elliptical with L_B is $17.5(\frac{L_B}{1.2 \times 10^{10} L_{B,\odot}})^{0.5} \times R_e$ (listed in the table) kpc.

^f The half-mass radius of MPCs in simulation units of R_d ($=17.5$ kpc). The real scale of this can be estimated in the same way as the above for R_e .

^g The half-mass radius of MRCs in simulation units of R_d ($=17.5$ kpc). The real scale of this can be estimated in the same way as the above for R_e .

^h The kinematic energy of a multiple merger is due totally to random motion of the five constituent galaxies.

ⁱ The kinematic energy of a multiple merger is due totally to rotational motion of the five constituent galaxies.

vertical velocity dispersion at a given radius is set to be half as large as the radial velocity dispersion at that point, as is consistent with the trend observed in the Milky Way (e.g., Wielen 1977).

The radial scale length of a disk and the maximum rotational velocity for the adopted mass profiles of dark matter, bulge, and disk is 3.5 kpc and 220 km s^{−1}, respectively, for the spiral with $M_d = 6.0 \times 10^{10} M_\odot$ and $R_d = 17.5$ kpc. The total mass of a disk galaxy is $10.17 \times M_d$ corresponding to $6.1 \times 10^{11} M_\odot$ for all models. These adopted values are consistent with those observed for the Galaxy (e.g., Binney & Tremaine 1987). Thus total mass of a merger remnant is $10.17(1+m_2)M_d$ (where m_2 is the mass ratio of merging two spirals) for a pair merger and $50.85M_d$ for a multiple merger. The details of these two different sets of merger models are described later.

2.2 Initial distributions and kinematics of MPCs and MRCs

The Galactic GCS and the stellar halo have similar radial density profiles of $\rho(r) \propto r^{-3.5}$ (van den Bergh 2000). We therefore assume that a GCS in a spiral has the following radial density profile:

$$\rho(r) = \frac{\rho_{gc,0}}{(a_{gc}^2 + r^2)^{1.75}}, \quad (2)$$

where r , $\rho_{gc,0}$, and a_{gc} are the spherical radius, the central number density of the GCS, and the scale length of the GCS, respectively. We adopt different values of a_{gc} for MPCs and MRCs where $\rho_{gc,0}$ is determined according to the adopted a_{gc} . The scale length is represented by a_{mpc} for MPCs and a_{mrc} for MRCs and the ratio of a_{mrc} to a_{mpc} is set to be 0.5 for most of models. This adopted value of 0.5 is reasonably consistent with observations (Forbes et al. 1997). The GCS with $a_{\text{mrc}} \sim 0.86R_d$ is consistent with the observed GC distribution of the Galaxy. The stellar halo in a spiral has the same distribution as MPCs in all models. The cut off radius (R_c) beyond which no GC (and stellar halo) particles are initially allocated is set to be $2R_d$ for MPCs and R_d for MRCs in the models with $a_{\text{mrc}}/a_{\text{mpc}} = 0.5$.

The GCS in a spiral is assumed to be supported purely by velocity dispersion and its dispersion is assumed to be isotropic. We therefore estimate the velocities of GC particles from the gravitational potential at the positions where they are located.

In detail, we first calculate the one-dimensional isotropic dispersion according to the (local) virial theorem:

$$\sigma^2(r) = -\frac{U(r)}{3}, \quad (3)$$

where $U(r)$ is the gravitational potential at the position r . Then we allocate a velocity to each GC particle so that the distribution of velocities of these particles has a Gaussian form with a dispersion equal to $\sigma^2(r)$.

Note that we use the above $U(r) - \sigma^2(r)$ relation rather than the Jeans equation for a spherically symmetric system (Binney & Tremaine 1987);

$$\frac{d(\rho(r)\sigma^2(r))}{dr} = -\rho(r)\frac{d\Phi(r)}{dr}. \quad (4)$$

This is firstly because the self-gravitating systems modeled in the present study are composed of six different stellar components (dark matter halo, $R^{1/4}$ -law bulge, stellar halo, disk, MPC, and MRC) with non-analytical radial density distributions and secondly because we introduce a cut off radius for each component. The derived $\sigma^2(r)$ at each location of a particle is consistent with those derived in the Jeans equation.

The total number of GCs (N_{gc}) for each spiral is 1000 (MPCs + MRCs). This is several times larger than those observed for the Galaxy or M31, and we adopt this number to improve the statistics on the measured kinematics. For example, the uncertainty in rotational velocity (V_{rot}) in each radial bin is estimated as $V_{rot}/\sqrt{2(N_i - 1)}$, where N_i is the total number of particles in each bin. This error is typically less than $\sim 20 \text{ km s}^{-1}$ in radial bins for the outer part of a merger remnant ($R \sim 20 \text{ kpc}$) in the models with $N_{gc} = 1000$. This uncertainty is smaller than V_{rot} ($\sim 60 \text{ km s}^{-1}$) such that we can place reasonable constraints on the rotational kinematics of GCs in merger remnants. For models with $N_{gc} = 100$, the error bar is comparable to V_{rot} so that it is at best challenging to derive any meaningful conclusions on GC kinematics. Clearly, we could have derived radial profiles of V_{rot} with better statistics for models with, for example, $N_{gc} = 10000$. However, such a GCS is consistent with only the most luminous cD galaxies. Thus 1000 GCs is a reasonable compromise between these two extremes.

Also, we stress here that we assume that both MPCs and MRCs are dynamically supported by velocity dispersion only: We do not intend to investigate the influence of initial rotation of GCSs on the final kinematics of GCSs in merger remnants. Statistical studies of the rotational properties of GCSs, in particular, MRCs, have not yet been performed for spiral galaxies. Given the fact that some MRCs in the Galaxy and M31 show rotational kinematics (e.g., Huchra et al. 1991), this assumption could be questionable for MRCs. Suffice to say that we leave investigations of the importance of initial rotation in GCSs to future studies.

The present study considers only the physical role of galaxy merging in determining kinematical properties of GCSs in an idealized manner, and does not attempt to address the origin of GC kinematics and S_N of giant ellipticals (e.g., M87 and NGC 1399) in the central regions of galaxy clusters. In such environments, accretion of GCs from cluster member galaxies can play a significant role in determining physical properties of GCSs (e.g., Bekki et al. 2003), and initial conditions based upon cosmological simulations are probably more appropriate. Cosmological simulations of GC formation in the early universe are still at the level where individual GCs are unresolved (e.g., Kravtsov & Gnedin 2003) such that there are still significant uncertainties in the predicted properties of GCSs of the progenitors of elliptical galaxies. Thus we consider our approach to be complementary to the current cosmological simulations.

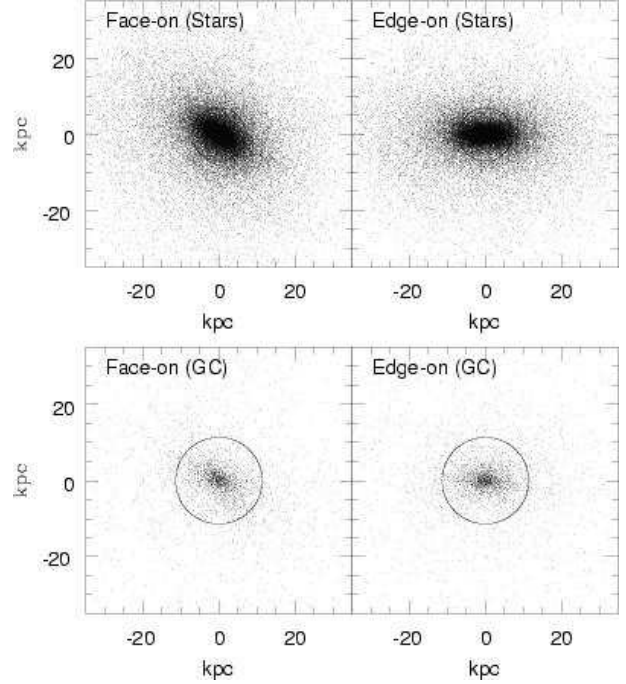


Figure 1. Stellar (upper panels) and globular cluster (lower panels) distributions projected onto the x - y plane (i.e., face-on view, left) and the x - z plane (i.e., edge-on view, right) for the merger remnant of the fiducial (PM1) model at $T = 4.5 \text{ Gyr}$, where T is time that has elapsed since the simulation starts. GCs in the lower two panels include both MPCs and MRCs and the circle in each panel represents the effective radius of each GC component.

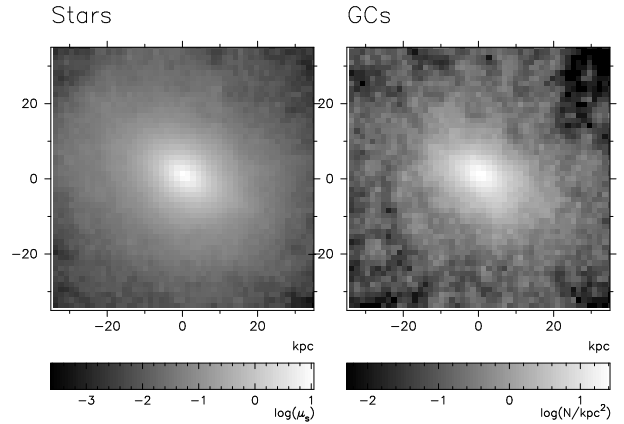


Figure 2. The 2D smoothed density distributions of stars (left) and GCs (right) projected onto the x - y plane for the fiducial model at $T = 4.5 \text{ Gyr}$. Both stellar and GC distributions appear to be similarly flattened.

2.3 Orbital configurations

2.3.1 Pair mergers

We investigate both a “pair merger” involving only two spiral galaxies and a “multiple merger” containing five galaxies. The multiple merger model for elliptical galaxy formation has been proposed (e.g., Barnes 1989; Weil & Hernquist 1994, 1996; Bekki 2001) to provide an evolutionary link between a small compact group of galaxies and an isolated

giant elliptical. For the pair merger model, the mass ratio of the two spirals (m_2) is assumed to be a free parameter. In all of the simulations of pair mergers, the orbit of the two disks is set to be initially in the xy plane and the distance between the center of mass of the two disks is assumed to be 6 in our units (corresponding to 105 kpc). The pericenter distance (r_p) and the eccentricity (e_p) in a pair merger are assumed to be free parameters that control orbital energy and angular momentum of the merger. The spin of each galaxy in a merger is specified by two angles θ_i and ϕ_i , where suffix i is used to identify each galaxy. θ_i is the angle between the z axis and the vector of the angular momentum of a disk. ϕ_i is the azimuthal angle measured from the x axis to the projection of the angular momentum vector of a disk onto the xy plane.

2.3.2 Multiple mergers

Each multiple merger model contains equal-mass spiral galaxies with random orientations of intrinsic spin vectors which are uniformly distributed within a sphere of size $6R_d$. The most important parameter in this multiple merger model is the ratio of the initial kinematic energy (T_{kin}) of the merger to that of initial potential (W). By varying this ratio (t_v ; defined as $|2T_{\text{kin}}/W|$) from 0.25 to 0.75, we investigate how t_v controls the final GC kinematics of the merger remnants. We show the results of two extreme cases: (1) where the initial kinetic energy of a multiple merger is due entirely to the random motion of the five constituent galaxies (referred to as “dispersion supported”) and (2) where it is due entirely to (rigid) rotational motion (“rotation supported”). These two cases enables us to understand how initial rotation (or dispersion) controls the resulting kinematical properties of GCs in merger remnants.

In total we have investigated 55 models of pair mergers, but only present the results of 18 models which illustrate representative results on GC kinematics. The time taken for the progenitor spirals to completely merge and reach dynamical equilibrium is less than 16.0 in our units (~ 2.2 Gyr) for most of our major merger models. The total number of particles is 112680 for a pair merger and 281700 for a multiple merger. Table 1 summarises the model parameters for each model:

Model number (column 1), the mass ratio m_2 (2), the orbital eccentricity e_p (3), the pericentre distance r_p (4), θ_1 (5), θ_2 (6), ϕ_1 (7), ϕ_2 (8), $a_{\text{mrc}}/a_{\text{mpc}}$ (9), t_v (10), R_e (11), $R_{e,\text{mpc}}$ (12), $R_{e,\text{mrc}}$ (13), and comments (14). The method of how to derive the half-mass radii of stars (R_e), MPCs ($R_{e,\text{mpc}}$), and MRCs ($R_{e,\text{mrc}}$) of the merger remnants are described in §2.5.

Although we adopt a larger number (2000) of GCs in merger progenitor spirals for the purpose of kinematical analysis with smaller error bars, the present results of kinematical properties do not depend on the number of initial GCs for $N_{\text{GC}} \geq 200$ (Note here that the error bars become significantly large for small $N_{\text{GC}} \sim 200$). As shown later, GCSs both in pair mergers and in multiple ones can have a significant amount of rotation in their outer parts. This is not due to the adopted large number of GCs and thus suggests that most merger remnants can have GCSs with a significant amount of rotation.

2.4 Methods for kinematical analysis

2.4.1 Radial gradients of V_{rot} and σ

In estimating radial profiles of V_{rot} and σ for a merger remnant projected onto a given plane (e.g., the x - y plane), we first rotate the remnant such that the major axis of the rotated stellar remnant coincides with the x -axis (or y -axis) in the projection. Then we estimate V_{rot} and σ of GCs at each radius along the major axis in each projection to obtain the radial profiles both for MPCs and MRCs. In estimating V_{rot} and σ at each radius, we adopt the same method as used by Peng et al. (2004a) with a slit width of $0.34R_d$. Radial profiles of V_{rot} and σ are estimated for $R \leq 6R_e$ beyond which uncertainties become excessive due to finite sampling.

2.4.2 Smoothed 2D density and velocity fields

We investigate the projected two-dimensional (2D) density and velocity distributions of a GCS in each merger model for $0 \leq R \leq 2R_e$, where R_e is the stellar effective radius of the merger remnant. Since each GCS is composed of 1000 GCs, we need to use smoothing methods to draw smoothly changing 2D density and velocity fields from these discrete data. Similar to Peng et al. (2004a,b) we use a 3D Gaussian kernel function with a smoothing length of 0.17 in our units (corresponding to 3 kpc) to smooth the velocity (density) field around each GC particle. We choose this smoothing length of 0.17, so that we can examine *global* 2D fields without losing resolution within R_e . The simulation field is divided into a 50×50 grid and the line-of-sight-velocity and velocity dispersion are estimated in each grid square.

2.4.3 Spin axis misalignment

We also examine possible kinematical differences between the dark matter halo, stars, MPCs, and MRCs for each merger remnant elliptical. In order to estimate kinematical differences, we first derive the normalized spin (angular momentum) vector for each component:

$$\mathbf{L}_{\text{DM}} = \frac{1}{C_{\text{DM}}} \sum_{i=1}^{N_{\text{DM}}} \mathbf{x}_i \times \mathbf{v}_i, \quad (5)$$

where N_{DM} , \mathbf{x}_i , \mathbf{v}_i , and C_{DM} are the total number of dark matter particles, the position vector of each dark matter particle, the velocity vector of the particle, and the constant to normalize the spin vector (thus equivalent to L_{DM}). The same procedure is used for estimating \mathbf{L}_S (for stars), \mathbf{L}_{MPC} , and \mathbf{L}_{MRC} . Based on these normalised spin vectors, the misalignment angle ($\Theta_{\text{DM-MPC}}$) between the dark matter halo and the MPCs may be estimated with the following formula:

$$\Theta_{\text{DM-MPC}} = \arccos(\mathbf{L}_{\text{DM}} \cdot \mathbf{L}_{\text{MPC}}) \quad (6)$$

The same formula is used for estimating $\Theta_{S-\text{MRC}}$ and $\Theta_{\text{DM-MRC}}$.

2.5 Half-mass radii of MPCs and MRCs

We investigate half-mass (or half-number) radii of MPCs and MRCs and compare them with the effective (or half-mass) radii of stars in ellipticals. We estimate R_e , $R_{e,\text{mpc}}$,

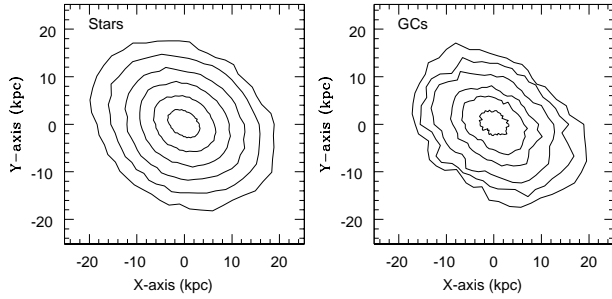


Figure 3. Density contours for the smoothed density profile of stars (left) and GCs (right) shown in Fig. 2. Note that the major axis of the stellar distribution is well aligned with that of the GCs. The outer isophotes of the GCs become irregular due to finite sampling.

and $R_{e,\text{mrc}}$ for stellar and GC particles that are within a radius of R_{cut} of a merger remnant in each model. We adopt $2R_d (=35 \text{ kpc})$ as a reasonable value for R_{cut} and the above effective radii depend only weakly on R_{cut} for $R_{\text{cut}} > R_d$. For example, R_e is 0.37 (6.5 kpc) for $R_{\text{cut}} = 2R_d$ and 0.29 (5.1 kpc) for $R_{\text{cut}} = R_d$.

In order to compare these effective radii with observations for ellipticals with *different luminosities*, the values of R_e , $R_{e,\text{mpc}}$, and $R_{e,\text{mrc}}$ are given in dimensionless units in the Table 1. For convenience, we also give r_e , $r_{e,\text{mpc}}$, and $r_{e,\text{mrc}}$ given in real scales (kpc) below.

By assuming a B -band mass-to-light ratio of 5 for the merger progenitor disks and adopting the observed relation between R_0 (disk scale length) and L_d ($L_d \propto R_0^2$; Freeman 1970), where L_d is the B -band total luminosity of a disk, we can derive the effective radius of stars (r_e) for an elliptical with the B -band luminosity of L_B in units of $L_{B\odot}$ from the value (R_e) listed in the Table 1 as follows:

$$r_e = 17.5 \left(\frac{L_B}{1.2 \times 10^{10} L_{B\odot}} \right)^{0.5} \times R_e \text{ kpc}. \quad (7)$$

For example, the elliptical in the fiducial model with $L_B = 1.2 \times 10^{10} L_{B\odot}$ (or $M_d = 6.0 \times 10^{10} M_\odot$) has r_e (real scale) of 6.5 kpc. $r_{e,\text{mpc}}$ and $r_{e,\text{mrc}}$ can be derived from $R_{e,\text{mpc}}$ and $R_{e,\text{mrc}}$ for a given M_d of a model in the same as r_e .

Future observational studies of the structural parameters of GCSs will allow $r_{e,\text{mpc}}$ and $r_{e,\text{mrc}}$ to be derived separately for nearby ellipticals, thereby probing the relative distributions of MPCs and MRCs with respect to stars of their host galaxies (e.g., Forte et al. 2005). Therefore, theoretical predictions on $r_{e,\text{mpc}}/r_e$ and $r_{e,\text{mrc}}/r_e$ are useful for interpreting these observational results.

3 RESULTS

3.1 The fiducial model

3.1.1 Spatial distributions of MPC and MRC

Fig. 1 shows the final mass distributions of stars and GCs of an elliptical galaxy formed by major merging at $T = 4.5 \text{ Gyr}$ in the fiducial model. Both stars and GCs show flattened distributions in the face-on and the edge-on views,

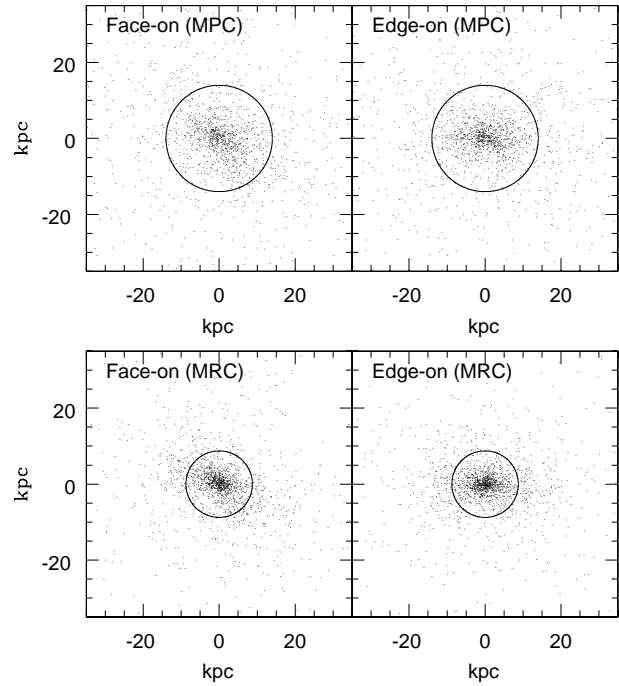


Figure 4. The same as Fig. 1 but for MPCs (upper panels) and for MRCs (lower panels). The major axis of the MPC distribution is well aligned with that of the MRCs both for the face-on and the edge-on views. This is an indication that intrinsic shapes of MPCs and MRCs are quite similar to each other. Note also that MRCs show more compact distribution than MPCs.

suggesting that the stars and GCs have intrinsically prolate-triaxial distributions. This result demonstrates that galaxy major merging can transform initially spherical distributions of GCs in spirals into moderately flattened distributions in remnant ellipticals. The half-mass radius of the GCSs in each projected distribution is a factor of 1.6 greater than that of the stars, and a factor of 2.6 smaller than that of the dark matter halo. The half-mass radius of the GCs in the merger remnant elliptical increases by only $\sim 14\%$ with respect to that in the progenitor spirals. This result implies that there may well be only marginal differences between the half-mass radii of spirals and ellipticals formed by major merging at a given luminosity.

Figs. 2 and 3 show, for the fiducial model, the smoothed distributions of stars and GCs (projected onto the x - y plane) and the isodensity contours of the distributions, respectively. These two figures clearly indicate the alignment of the major axes between the stellar distribution and the GCs. The difference in position angles of the smoothed distributions is only ~ 10 degrees at the stellar effective radius (R_e): *The aligned major axis between stars and GCs appears to be one of the principal characteristics of ellipticals formed by major merging.* The ellipticity of stars (ϵ_s) and GCs (ϵ_{gc}) at R_e is 0.18 and 0.22 respectively, indicating that the GC distribution is slightly more flattened than the stellar one. The stellar distribution shows a near constant ellipticity (~ 0.2) for $R > R_e$ whereas the GCs show weak radial dependencies of the ellipticity, with a slight increase (~ 0.3) at larger radii ($R = 3R_e$). These results are due to the similarity in *intrinsic* mass distributions between the stars and GCs, such that they do not depend on viewing angle (i.e., projection). This

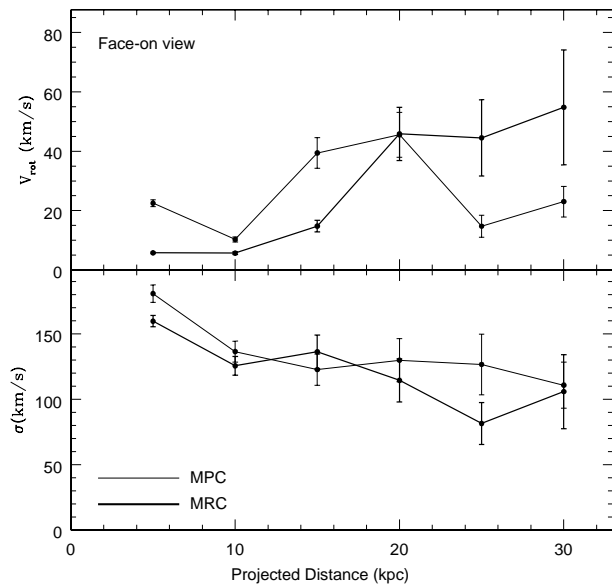


Figure 5. Radial profiles of rotational velocity V_{rot} (upper panel) and velocity dispersion σ (lower panel) for MPCs (thin solid) and for MRCs (thick solid) in the fiducial model projected onto the x - y plane (face-on view) at $T = 4.5$ Gyr. Both MPCs and MRCs show a significant rotation for $R > 20$ kpc.

alignment between stars and GCs is broadly consistent with observations for nearby elliptical galaxies (e.g., Forbes et al. 1996).

Fig. 4 clearly demonstrates that (1) the 2D distributions of MPCs and MRCs are similar to each other in the sense that both distributions are flattened along the major axis of stars in both x - y and x - z projection, (2) the major axes of the distributions of MPCs and MRCs are nearly coincident with that of the stars, and (3) MRCs have a more compact (by a factor of 1.6) distribution than MPCs. We confirm that major-axes alignment between stars, MPC, and MRCs can be also seen. The GC distribution is more flattened for MPCs ($\epsilon_{\text{gc}} \sim 0.3$) than MRCs ($\epsilon_{\text{gc}} \sim 0.2$) within R_e , although there is no significant difference between the two outside R_e . Thus we conclude that the flattened spatial distributions of MPCs are expected to be characteristics of elliptical galaxies formed in dissipationless major galaxy merging.

3.1.2 Kinematics

Fig. 5 shows the radial dependencies of rotational velocity (V_{rot}) and velocity dispersion (σ) along the major axis of the stellar distribution projected onto the x - y plane (“face-on view”) for MPCs and MRCs in the fiducial model. The rotation curves do not increase monotonically, but V_{rot} at $R \sim 20$ kpc is significantly greater than that at $R \sim 10$ kpc for both GC subpopulations. Given the fact that GCs in the progenitor spirals are given no net rotation initially, these results demonstrate that outer GCs in the merger remnant ellipticals can exhibit rotation due to the redistribution of angular momentum. The amount of rotation in the GCs is relatively modest, with $V_{\text{m}}/\sigma_0 = 0.25$ for MPCs and 0.34 for MRCs. Both MPCs and MRCs show radially decreas-

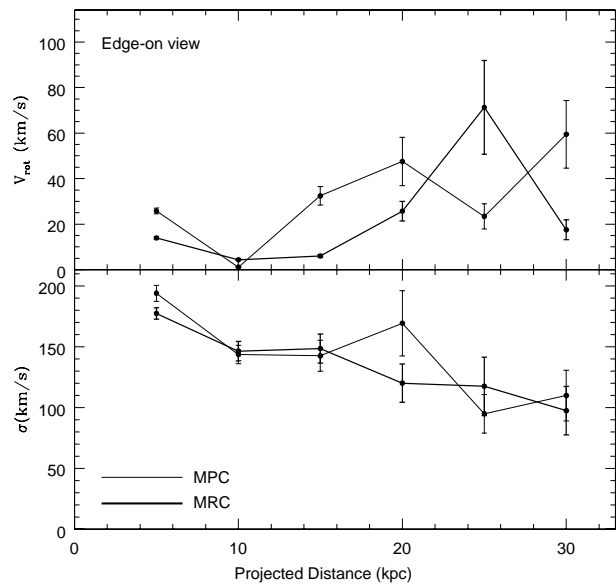


Figure 6. The same as Fig. 5 but for the x - z projection (edge-on view).

ing profiles of σ with no significant differences in the radial profiles between the two GC populations.

As shown in Fig. 6, the simulated radial dependencies of V_{rot} are broadly similar between the two different projections (i.e., the x - y and the x - z planes). The apparent independence of global V_{rot} profiles on projection suggests that moderate rotation ($30 \sim 40 \text{ km s}^{-1}$) in the outer halo regions ($R > 20$ kpc) is a common characteristic of GC kinematics in major merger remnant ellipticals.

The radial profiles of σ for MPCs do not significantly differ from that of MRCs, which probably reflects the fact that the two GC subpopulations follow the same gravitational potential in the elliptical. V_{m}/σ_0 and the slope of the σ profile for each GC population is slightly different between the two different projections (e.g., $V_{\text{m}}/\sigma_0 = 0.25$ for the x - y projection and 0.3 for the x - z one in MPCs). The difference of the slopes of the σ profiles are a result of the anisotropic velocity dispersion profiles of the remnant.

Figs. 5 and 6 also show that the central velocity dispersion (σ_0) of MPCs is slightly higher (dynamically hotter) than that of MRCs. The ratio of the dark matter to GCs σ_0 is ~ 1.05 (1.01) for MPCs and 1.20 (1.11) for MRCs in the face-on (edge-on) view. This suggests that an estimation of the total mass of the elliptical, by using the central velocity dispersion data of the GCs and the virial (or Jeans) theorem, may lead to an underestimate of the total mass of the elliptical by up to 40 %. Thus, in principle, kinematical data of MPCs in an elliptical allow for a more reliable mass estimation of the elliptical than MRCs. The σ_0 of MPCs reflects that of the underlying dark matter more effectively than the MRCs.

Since the 2D velocity and velocity dispersion fields of the GCS will be given in our forthcoming papers (Bekki et al. 2005), we here briefly summarize the main results of these. Firstly, both minor axis and major axis rotation can be seen in MPCs and MRCs. Secondly, the direction of the rotation along the major axis for the dark matter halo is the same as those for MPCs and MRCs, which suggests that observations

of GC kinematics in an elliptical galaxy can indirectly probe the kinematics of the dark matter halo. Thirdly, the 2D σ distribution appears to be more flattened in MRCs than in MPCs, the direction of the flattening of MRCs is the same as that of stellar density distribution and appears to differ from that of MPCs, and substructure is evident (i.e., local maxima of σ) for both MPCs and MRCs.

3.1.3 Summary of generic results

GCSs of merger remnants in pair merger models have the following generic properties: (1) well aligned major axes between stars, MPCs, and MRCs, (2) a larger amount of intrinsic angular momentum in the outer part of galaxies both for MPCs and for MRCs, (3) negative radial gradients of σ , (4) flattened 2D distributions of velocity dispersion, and (5) rather complicated distributions of line-of-sight-velocity fields. Physical properties other than the above, such as the ellipticity of 2D number distributions, the slopes of radial V_{rot} and σ profiles, and the details of the velocity ellipsoids of GCSs, are model-dependent, as described below.

3.2 Parameter dependencies

3.2.1 Orbital configurations of major merging

It is important to ask: how do different orbital configurations effect the final kinematic properties of the GC system? In the following, we summarize these dependencies.

(1) Irrespective of initial orbits, both MPCs and MRCs in the merger remnant ellipticals show moderate amounts of rotation in their outer halo regions ($R > 20$ kpc). $V_{\text{rot}}(r)$, σ , V_{m} , and V_{m}/σ_0 all depend on the orbital configuration. Radial V_{rot} profiles can differ between MPCs and MRCs for a given projection.

(2) All major merger models show σ decreases as a function of radius, with the slope depending on projection and orbital configuration. There are no significant differences in the σ profiles between MPCs and MRCs in our models.

(3) MPCs and MRCs generally show both major- and minor-axis rotation in the 2D V_{los} distributions. MPCs and MRCs in most models show quite flattened 2D σ distributions, which reflect the fact that for most merger remnants, the GCS have anisotropic velocity dispersions.

(4) Both MPCs and MRCs in ellipticals formed from major merger models with prograde-prograde orbital configurations show *figure rotation* with slow pattern speeds. Since dark matter halos in these models also show figure rotation, this suggests that kinematical studies of MPCs and MRCs in ellipticals could in principle test for global figure rotation in their dark matter halos.

(5) V_{m}/σ_0 of MPCs differs for models with different orbital configurations. In addition, V_{m}/σ_0 can be significantly different between stars, MPCs, and MRCs in a given galaxy. For example, Fig. 7 shows that V_{m}/σ_0 of MPCs and MRCs in ellipticals are significantly larger than that of the main stellar bodies (within $2R_e$) in nearly all models. This is a natural result of the outer GCs containing a larger amount of intrinsic angular momentum.

(6) Fig. 8 shows that the outer stellar halos ($R = 6R_e$) of ellipticals formed from major merging have nearly the same

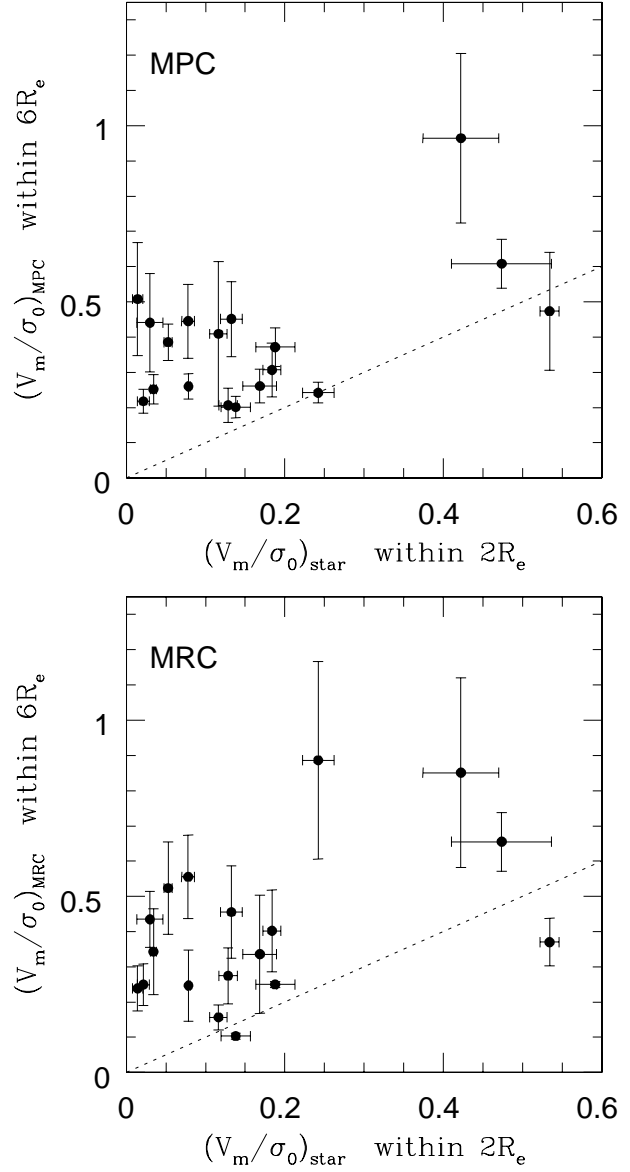


Figure 7. Locations of six major merger models (PM 1 – 6) on the $(V_{\text{m}}/\sigma_0)_{\text{star}}$ - $(V_{\text{m}}/\sigma_0)_{\text{MPC}}$ plane (upper panel) and on the $(V_{\text{m}}/\sigma_0)_{\text{star}}$ - $(V_{\text{m}}/\sigma_0)_{\text{MRC}}$ plane (lower panel). Here three results for three different projections are derived for each merger model so that 18 results are shown in each panel. $(V_{\text{m}}/\sigma_0)_{\text{star}}$ is estimated for $R \leq 2R_e$ whereas $(V_{\text{m}}/\sigma_0)_{\text{MPC}}$ and $(V_{\text{m}}/\sigma_0)_{\text{MRC}}$ are estimated for $R \leq 6R_e$. The dotted line draws a boundary above which $(V_{\text{m}}/\sigma_0)_{\text{MPC}}$ (or $(V_{\text{m}}/\sigma_0)_{\text{MRC}}$) is larger than $(V_{\text{m}}/\sigma_0)_{\text{star}}$.

values of V_{m}/σ_0 as those of MPCs and MRCs. This result implies that if ellipticals are formed by major merging, there should be no significant differences in V_{m}/σ_0 between stellar halos and other kinematic tracers such as PNe or GCs.

(7) Fig. 9 demonstrates that there is a weak correlation between V_{m}/σ_0 within $2R_{\text{eff}}$ and $6R_{\text{eff}}$ for MPCs in the sense that MPCs with larger V_{m}/σ_0 within $2R_{\text{eff}}$ show larger V_{m}/σ_0 within $6R_{\text{eff}}$. If the main stellar body of a merger remnant can obtain larger angular momentum during galaxy merging (thus larger V_{m}/σ_0 within $2R_{\text{eff}}$), then the outer halo of the remnant can probably also obtain larger angular momentum (thus larger V_{m}/σ_0 within $6R_{\text{eff}}$). The

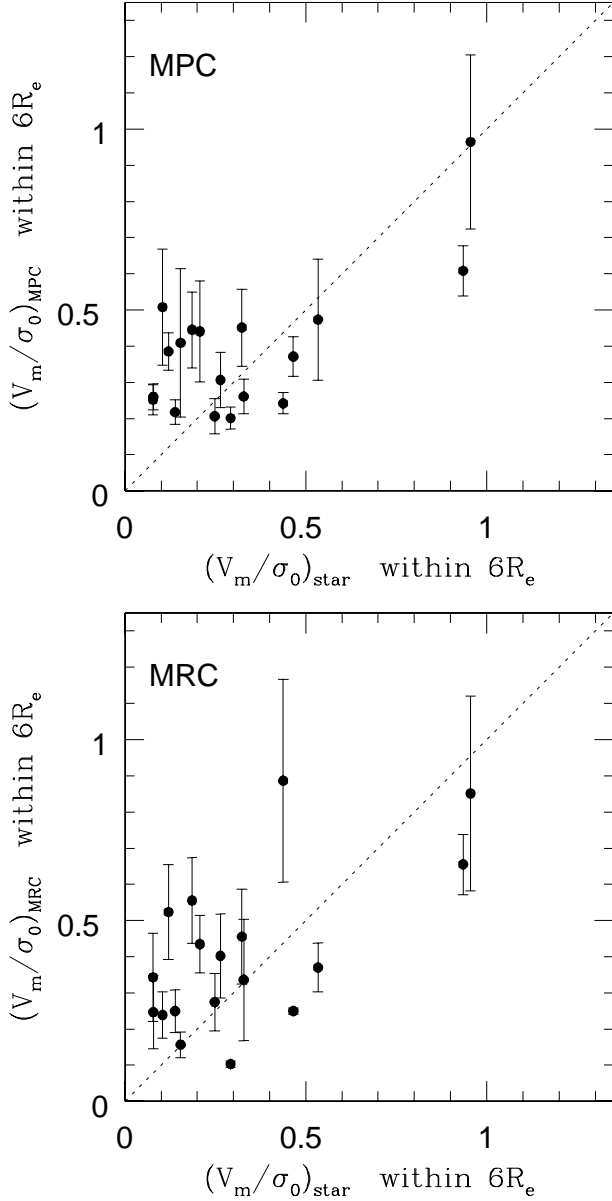


Figure 8. The same as Fig. 7 but for $(V_m/\sigma_0)_{\text{star}}$ estimated for $R \leq 6R_e$.

weak trend seen in MPCs is not so clear in MRCs. V_m/σ_0 is larger in the outer regions for both MPCs and for MRCs in nearly all merger models.

(8) The major-axes of MPCs and MRCs nearly coincides with that of stars in each of the major merger models. This suggests that future observations on *global distributions of GCs throughout the entire halo regions of elliptical galaxies* enable us to test the merger scenario of elliptical galaxy formation. Kinematics of MPCs and MRCs in each model is strikingly similar to that of the dark matter halo, which strongly suggests that GCs can be regarded as tracers of kinematics of dark matter halos.

3.2.2 Mass ratios (m_2)

The dependencies of kinematical properties of MPCs and MRCs on the mass ratios (m_2) of major merging are

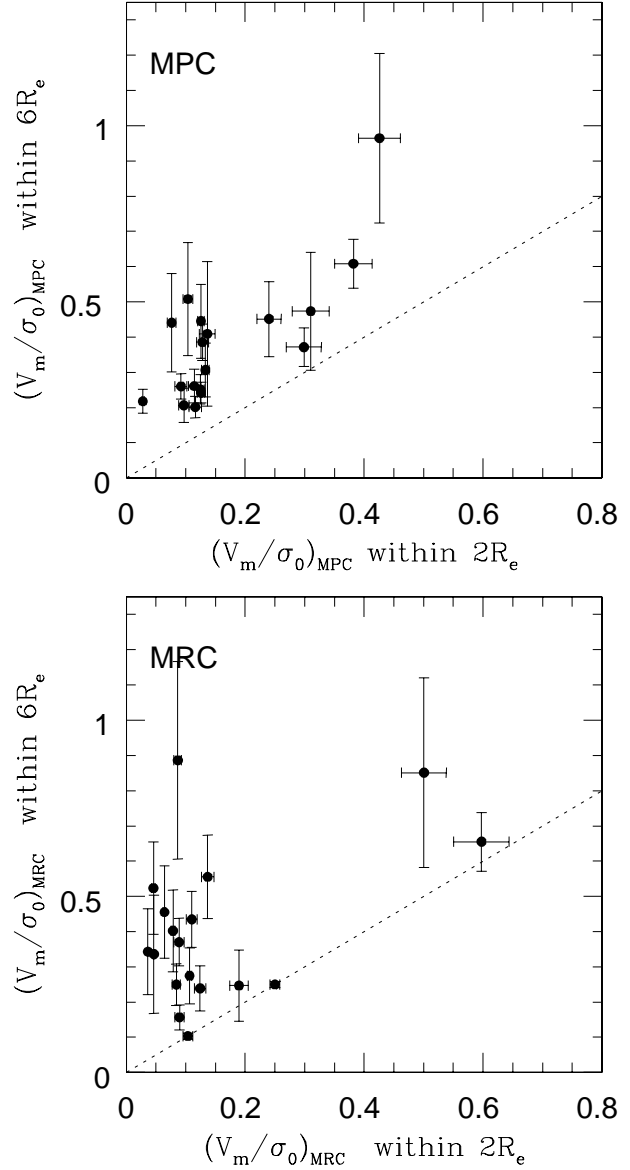


Figure 9. Correlations between $(V_m/\sigma_0)_{\text{MPC}}$ estimated for $R \leq 2R_e$ and those for $R \leq 6R_e$ (upper) and between $(V_m/\sigma_0)_{\text{MRC}}$ estimated for $R \leq 2R_e$ and those for $R \leq 6R_e$ (lower). These correlations are derived from 18 results of 6 major merger models with three different projections.

summarized as follows.

(1) The spatial distributions of MPCs and MRCs are more flattened in models with larger m_2 for a given orbital configuration and projection. For minor merger models with $m_2 = 0.1$, galaxy merging can not significantly transform an initially spherical GC distribution into a flattened one due to weak tidal perturbation. Figs. 10 and 11 show examples of the dependence of final GC spatial distribution on the mass ratio. The ellipticity of the GCS (ϵ_{gc}) projected onto the x - z plane at R_e is 0.08 for $m_2 = 0.1$ and 0.20 for $m_2 = 1.0$ for this nearly prograde-prograde configuration.

(2) Stellar distributions of galaxies become more spherical (i.e., smaller stellar ellipticity ϵ_s) for larger m_2 , whereas the GCSs become more flattened (larger ϵ_{gc}). Therefore,

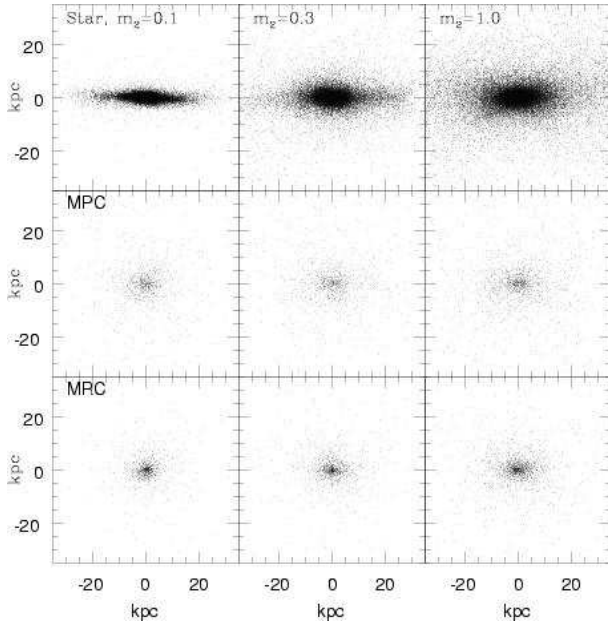


Figure 10. Final spatial distributions of stars (top), MPCs (middle), and MRCs (bottom) for three different merger models (PM7, 8, and 9): $m_2 = 0.1$ (left), $m_2 = 0.3$ (middle), and $m_2 = 1.0$ (right).

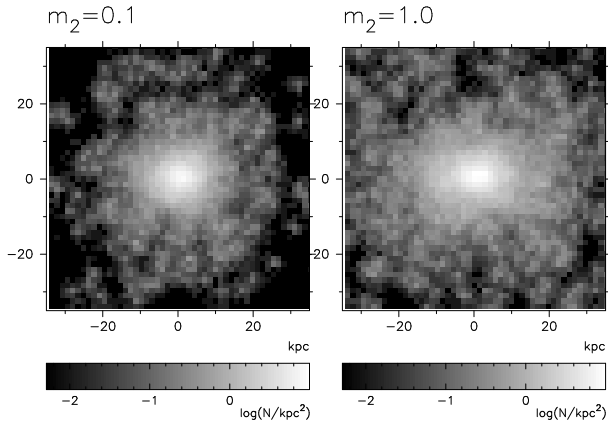


Figure 11. Smoothed density distributions of MPCs projected onto the x - z plane for $m_2 = 0.1$ (left) and $m_2 = 1.0$ (right).

more flattened early-type galaxies (e.g., S0s) may show smaller ϵ_{gc}/ϵ_s . It has been argued that minor or unequal-mass mergers of spirals can become S0s (e.g., Bekki 1998), and a statistical study of ϵ_{gc}/ϵ_s can test this hypothesis.

(3) MRCs in flattened early-type galaxies formed by mergers with small m_2 (~ 0.1) show a smaller amount of rotation (i.e., $V_m/\sigma_0 \sim 0.1$) when compared with MPCs. Fig. 12 shows an example of this V_{rot} difference between MPCs and MRCs in a merger model with $m_2 = 0.1$ in which the remnant looks like an S0. This difference is smaller for models with larger m_2 . These results imply that more flattened early-type galaxies are likely to show larger V_{rot} in MPCs than in MRCs. Initial results for the GC kinematics of the S0 NGC 524 support the notion that these galaxy types may result from minor/unequal-mass merging of spirals (Beasley et al. 2004).

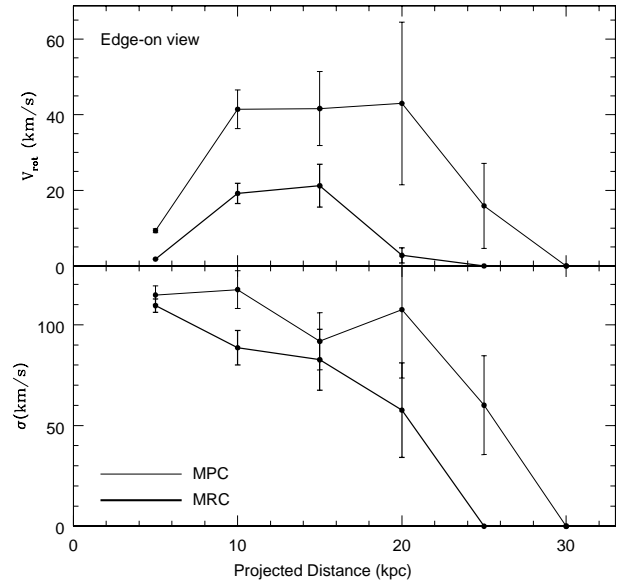


Figure 12. The same as Fig.5 but for the model with $m_2 = 0.1$ (PM7).

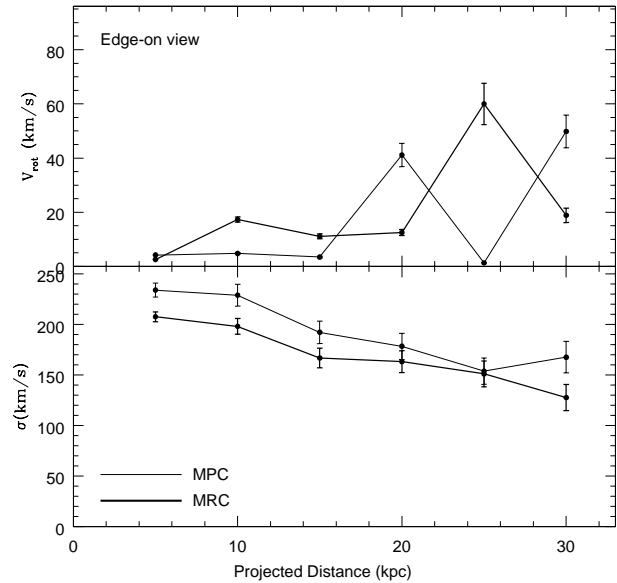


Figure 13. The same as Fig.5 but for the multiple merger model MM1.

(4) The radial gradients of σ are more likely to be steeper for early-type galaxies formed by mergers with smaller m_2 . V_{rot} of MPCs and MRCs of E/S0 merger remnants with small m_2 reaches a maximum in the inner parts of their host galaxies. Independent of m_2 , MPCs show larger velocity dispersions than MRCs, which implies that MPCs in early-type galaxies are *in general* dynamically hotter systems than MRCs.

3.2.3 Multiple mergers

Most of the results for multiple merger models (MM 1 – 6) are essentially the same as those obtained for pair merger

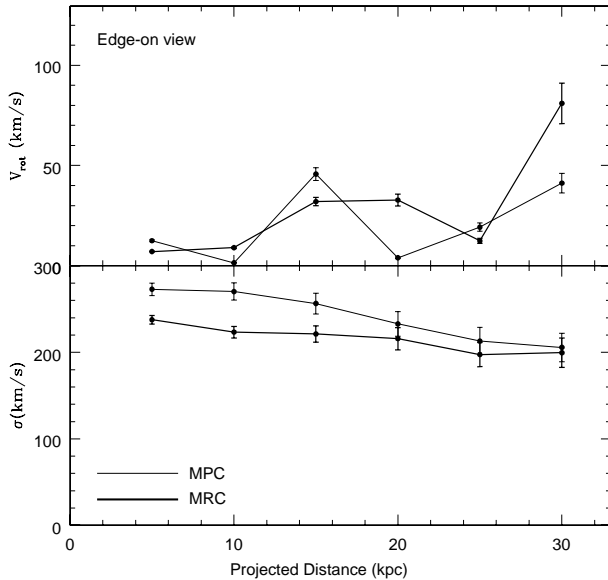


Figure 14. The same as Fig.5 but for the multiple merger model MM4.

ones. We thus summarize the salient dependencies in multiple merger models.

(1) Major-axis alignment between MPCs, MRCs, and stars in their projected 2D distributions can be seen in all models. The half-number radii of GCSs in ellipticals formed by multiple merging are a factor of ~ 1.3 larger than those formed by pair merging. Both MPCs and MRCs show flattened 2D distributions in all multiple merger models.

(2) Both MPCs and MRCs show significant amounts of rotation in the halo regions ($20 < R < 30$ kpc) of their host galaxies. Independent of model parameters, MPCs show larger σ than MRCs. Fig. 13 shows an example of the present model showing these general trends in GC kinematics of ellipticals formed by multiple merging. V_m/σ_0 is generally larger in ellipticals formed by multiple mergers initially having global rotation (i.e., MM4, 5, and 6) than those initially having no net rotation (i.e., MM1, 2, and 3).

(3) Some remnant ellipticals show flattened radial σ profiles within $2R_e$ (~ 20 kpc). Fig. 14 shows the result of the model MM4, in which both MPCs and MRCs have quite flattened σ profiles. These flattened σ profiles are not evident in pair merger models and may be regarded as one of the characteristics of multiple merger models. Such flattened σ profiles seen in some Es (e.g., NGC 4472; Côte et al 2003) could be understood in terms of multiple galaxy merging.

(4) Figs. 15 and 16 shows the radial V_{rot} and σ profiles of all pair and multiple merger models with three different projections, respectively. Although the total mass of the merger remnants in pair merger models are the same, *both the projected V_{rot} and σ profiles* are quite diverse. This is true for the multiple merger models. These results indicate that in deriving total masses of ellipticals using GC kinematics (i.e., radial V_{rot} and σ profiles) and the Jeans equation (Binney & Tremaine 1987), more careful dynamical analysis and physical interpretations should be done. In particular, the diverse V_{rot} profiles of GCSs imply that the contribution

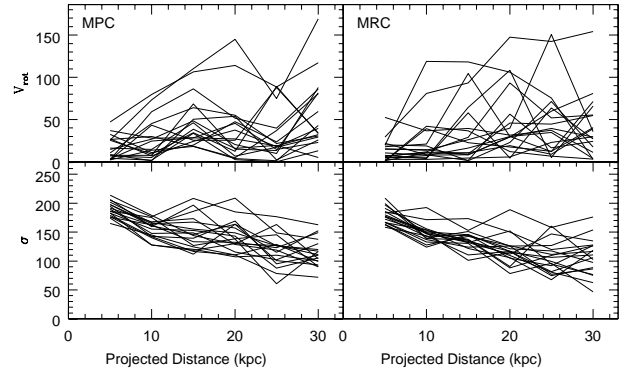


Figure 15. Radial profiles of V_{rot} (upper two) and σ (lower two) for MPC (left) and MRC (right) in the six pair major merger models (PM 1 – 6) with three different projections. In total 18 model results are given in each frame.

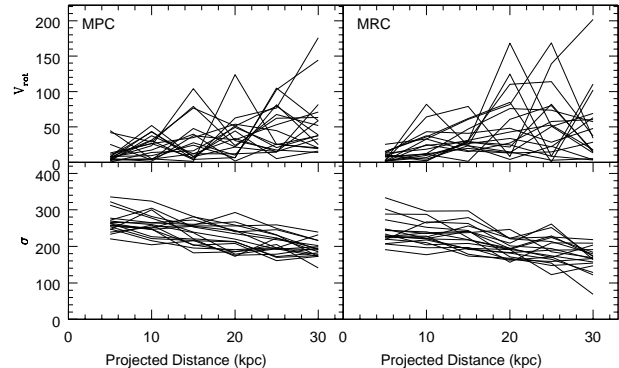


Figure 16. The same as Figure 15 but for the six multiple major merger models (MM 1 – 6) with three different projections. In total 18 model results are given in each frame.

of global rotation should be included in the mass estimation based on the Jeans equation.

(5) Figs. 15 and 16 also confirm that radial σ profiles are in general flatter in multiple merger models than in pair mergers both for MPCs and MRCs. Some pair and multiple merger models show significant rotation in MPCs: V_m/σ_0 ranges from 0.2 to 1.0. In this regard, it is interesting to consider the Milky Way, in which the MPCs have a net rotation of $\sim 60 \text{ km s}^{-1}$ (Freeman 1985). This corresponds to $V_m/\sigma_0 = 0.47$ for $V_m = 220 \text{ km s}^{-1}$ and $\sigma_0 \simeq V_m/\sqrt{3}$. The above result suggests that some Es have MPCs that rotate more rapidly than their counterparts in late-type spirals.

4 DISCUSSION

4.1 Kinematical differences of GCSs in cluster and field ellipticals

Previous numerical studies have shown that tidal stripping of GCs from cluster members, by the cluster global tidal field and galaxy-galaxy interactions, are important physical processes in the evolution GCSs in cluster galaxies (e.g., Muzzio 1987). Recent more sophisticated numerical studies (Bekki et al. 2003) have shown that more than 50 % of GCs initially within a cluster E can be stripped by cluster tidal fields (resulting in a lower S_N). Local S_N (i.e., S_N at a given

Table 2. Characteristics of GCSs in early-type galaxies formed from different types of galaxy mergers

Merger type	Host morphology	GCS structure	GCS kinematics
Major	E	More flattened	Rotation at larger r
Minor/unequal-mass	Flattened E/S0	More spherical	Little rotation at larger r

radius) can be reduced even further due to efficient tidal stripping of GCs in the outer parts of Es. The present study has demonstrated that GCs in the outer parts of Es formed by major merging have a significant amount of rotation and thus show large V_m/σ_0 .

Therefore, the logical conclusion from the present and previous works is that GCSs of cluster Es are likely to have lower V_m/σ_0 than those of field Es owing to the selective stripping of outer GCs in the cluster environment, *if both Es were formed by major galaxy merging*. Such differences are expected to be most clearly seen in field and cluster Es that are not located in the centers of their host clusters, since the GCSs of cD galaxies may have been influenced by several “secondary” physical processes such as GC accretion from cluster member galaxies and minor merging of dwarfs with GCs, after their formation.

4.2 Origin of S0s

The question of how and when red S0 galaxies formed in the field and in clusters remains an outstanding problem in astrophysics. Morphological and spectroscopic observations indicate that there is a smaller fraction of S0 galaxies in clusters of galaxies at $z \sim 0.4$ than locally (Dressler et al. 1997; Couch et al. 1998). This, combined with the increased fraction of blue late-type spirals in some distant clusters (e.g., Butcher & Oemler 1978), suggest that some mechanism drives strong evolution from blue spirals into red S0s in the course of cluster evolution.

The proposed theoretical models for S0 formation are ram pressure stripping (Farouki & Shapiro 1980), tidal compression by the gravitational field of clusters (Byrd & Valtonen 1990), tidal truncation of gas replenishment (Larson, Tinsley, & Caldwell 1980), and galaxy mergers (Bekki 1998). Although theoretical studies of the spectrophotometric evolution of S0s (e.g., Shioya et al. 2002, 2004) and on the morphological transformation processes of spirals in clusters (Bekki et al. 2001, 2002) have tried to identify the origin of cluster S0s, it remains unclear which model can best explain the observations.

The present study suggests that GC kinematics of S0s can provide a fresh clue to their origin. Our simulations have demonstrated that if S0s are formed by minor/unequal-mass merging, then MPCs and MRCs will show different kinematics when compared with those of their progenitor spiral. In particular, a significant amount of rotation in MPCs and larger V_m/σ_0 in MPCs than in MRCs appears to be principal characteristics of GCSs in S0s formed by such merging. Other cluster-related physical processes such as ram pressure stripping and tidal truncation of gas replenishment will not change the outer dynamical properties of GCSs in S0 progenitor spirals, so that GCSs of S0s formed entirely by these processes will not show any net rotation. It would also

be difficult for the GCSs of the S0 progenitors to be imparted with a net rotation if tidal compression by the gravitational field of clusters transforms spirals into S0s. Future kinematical studies of GCSs in the field and in clusters can potentially unravel the postulated different formation processes between field and cluster S0s.

5 CONCLUSIONS AND SUMMARY

We have numerically investigated the kinematic properties of GCSs in E/S0s formed by dissipationless galaxy merging. The dynamical evolution of metal-poor GCs (MPC) and metal-rich GCs (MRC), initially associated with the merger progenitor spirals, is followed and their resulting kinematics examined. We summarize our principle result as follows.

(1) Both MPCs and MRCs are expected to have significant amounts of rotation in Es formed by major galaxy merging with mass ratios (m_2) ~ 1 . This remains true even if the MPCs and MRCs initially have no net rotation in the progenitor spirals. This arises because the GCs obtain angular momentum with respect to their host galaxies during merging owing to the conversion of orbital angular momentum into intrinsic angular momentum of the remnants, particularly in the outer regions of the mergers. Both MPCs and MRCs show positive radial gradients of rotational velocity (V_{rot}) in the sense that outer parts of GCSs in Es ($R > 2R_e$) show larger V_{rot} than the inner parts ($R \sim R_e$).

(2) MPCs show slightly larger central velocity dispersion than MRCs for most major merger models, which indicates that MPCs are dynamically hotter stellar systems than MRCs. Velocity dispersion is likely to be higher in MPCs than in MRCs at any radius in ellipticals.

(3) V_m/σ_0 , where V_m and σ_0 are the maximum rotational velocity and the central velocity dispersion of a GCS, respectively, range from 0.2 to 1.0 for MPCs and from 0.1 to 0.9 for MRCs within $6R_e$ of Es formed by major merging. The distributions of V_m/σ_0 are similar between these two GC populations. For most major merger models, V_m/σ_0 of GCSs within $6R_e$ is greater than that of stars of Es within $2R_e$. MPCs (and MRCs) with larger V_m/σ_0 for $R \leq 2R_e$ show larger V_m/σ_0 for $R \leq 2R_e$. This correlation in GC kinematics between the inner and outer regions of Es is a natural result of global dynamical relaxation and angular momentum transfer, and in principle provides a test for the major merger scenario of elliptical galaxy formation.

(4) Radial profiles of V_{rot} for MPCs and MRCs are diverse, and are sensitive to orbital configuration, m_2 , and the viewing angle. Radial profiles of V_{rot} can differ between MPCs and MRCs which reflects the fact that the dynamical evolution of GCs during major merging depend on the GCs’ initial distribution. The negative radial gradients in velocity dispersion of MPCs and MRCs can also differ for

different model parameters. However, there are no significant differences in the profiles between MPCs and MRCs in the remnant elliptical.

(5) Outer MRCs in flattened early-type galaxies (e.g., S0s) formed by merging with small mass ratios ($m_2 \sim 0.1$) do not show any significant rotation. Furthermore, V_m is likely to be larger in MPCs than in MRCs for these flattened systems. These results suggest that the kinematic properties of GCSs in S0s can be quite different from those in Es. The V_{rot} in S0 galaxies obtain their peak values in their inner regions. The fundamental characteristics of GCSs in E/S0s formed from different mergers are summarized in Table 2.

(6) 2D distributions of line-of-sight-velocities of GCSs can be useful for examining global differences in kinematics between MPCs and MRCs. Both MPCs and MRCs show rotation along the minor- and major-axes of their host E for most major merger models. The general patterns of the 2D velocity fields are similar to each other between MPCs and MRCs.

(7) 2D velocity dispersion fields of GCSs in Es formed by major merging show flattening both in MPCs and in MRCs. This result is a clear indication of an anisotropic velocity dispersion in the GCSs, and demonstrates that major merging processes can change an initially isotropic velocity dispersion in the GCSs of spirals into an anisotropic one in the GCSs of Es. The direction of flattening appears to be similar between the two GC populations in Es.

(8) Kinematic properties of GCSs in Es formed by multiple major merging are generally similar to those of GCSs in Es formed by pair merging. However, a significant difference in GC kinematics between the two merger types is that very flattened radial σ profiles are only seen in Es formed by multiple merging. The major axis of the GCS distribution is nearly coincident with that of the stellar distribution in an E formed from both pair and multiple mergers

(9) Kinematic properties of MPCs in Es are similar to those of the surrounding dark matter halos, which implies that MPCs are a good probe of the kinematics of dark halos. This similarity in kinematics suggests that dynamical processes of major galaxy merging (i.e., violent relaxation and angular momentum redistribution) can align the spin axis of the GCS with those of the parent galaxy halo.

6 ACKNOWLEDGMENT

We are grateful to the anonymous referee for valuable comments, which contribute to improve the present paper. KB and DAF acknowledge the financial support of the Australian Research Council throughout the course of this work. The numerical simulations reported here were carried out on GRAPE systems kindly made available by the Astronomical Data Analysis Center (ADAC) at National Astronomical Observatory of Japan (NAOJ). This work was supported by NSF grant AST 02-06139.

REFERENCES

- Ashman, K. M., & Zepf, S. E., 1998, *Globular Cluster Systems* (Cambridge university press)
- Barnes, J. E., 1989, *Nature*, 338, 123
- Beasley, M. A., Baugh, C. M., Forbes, D. A., Sharples, R. M., & Frenk, C. S. 2002, *MNRAS*, 333, 383
- Beasley, M. A., Forbes, D. A., Brodie, J. P., Kissler-Patig, M., 2004, *MNRAS*, 347, 1150
- Bekki, K., 1998, *ApJ*, 502, L133
- Bekki, K., 2001, *ApJ*, 546, 189
- Bekki, K., & Shioya, Y. 1998, *ApJ*, 497, 108
- Bekki, K., & Couch, W. J., Shioya, Y., 2001, *PASJ*, 53, 395
- Bekki, K., Forbes, D. A., Beasley, M. A., Couch, W. J., 2002, *MNRAS*, 335, 1176
- Bekki, K., & Chiba, M., 2002, *ApJ*, 566, 245
- Bekki, K., & Couch, W. J., Shioya, Y., 2002, *ApJ*, 577, 651
- Bekki, K., Forbes, D. A., Beasley, M. A., Couch, W. J., 2003, *MNRAS*, 344, 1334
- Bridges, T., Beasley, M., Faifer, F., Forbes, D., Forte, J., Gebhardt, K., Hanes, D. Sharples, R., Zepf, S., 2003, in *Extragalactic Globular Clusters and their Host Galaxies*, 25th meeting of the IAU, Joint Discussion 6.
- Brodie, J. P., Schroder, L. L., Huchra, J. P., Phillips, A. C., Kissler-Patig, M., & Forbes, D. A., 1998, 116, 691
- Brodie, J. P. et al. 2004 in preparation
- Butcher, H. Oemler, A., 1978, *ApJ*, 219, 18
- Byrd, G., Valtonen, M., 1990, *ApJ*, 350, 89
- Cohen, J. G. & Ryzhov, A. 1997, *ApJ*, 486, 230
- Côte, P., Marzke, R. O., West, M. J., 1998, *ApJ*, 501, 554
- Côte, P., McLaughlin, D. E., Hanes, D. A., Bridges, T. J., Geisler, D., Merritt, D., Hesser, J. E., Harris, G. L. H., Lee, M. G., 2001, *ApJ*, 559, 828
- Côte, P., McLaughlin, D. E., Cohen, J. G., Blakeslee, J. P., 2003, *ApJ*, 591, 850
- Couch, W. J., Barger, A. J., Smail, I., Ellis, R. S., Sharples, R. M., 1998, 497, 188
- Dressler, A., Oemler, A., Couch, W. J., Smail, I., Ellis, R. S., Barger, A., Butcher, H., Poggianti, B. M., Sharples, R. M., 1997, *ApJ*, 490, 577
- Eggen, O. J., Lynden-Bell, D., Sandage, A. R. 1962, *ApJ*, 136,
- Farouki, R., Shapiro, S. L., 1980, *ApJ*, 241, 928
- Forbes, D. A. Franx, M., Illingworth, G. D., Carollo, C. M., 1996, *ApJ*, 467, 126
- Forbes, D. A., Brodie, J. P., Grillmair, C. J., 1997, *AJ*, 113, 1652
- Forte, J. C., Faifer, F., Geisler, D., 2005, *MNRAS*, 357, 56
- Freeman, K. C., 1985, in *The Milky Way Galaxy; Proceedings of the 106th Symposium*, ed. Dordrecht, D.Reidel Publishing Co., 1985, p113.
- Grillmair, C. J., Freeman, K. C., Bicknell, G. V., Carter, D., Couch, W. J., Sommer-Larsen, J., & Taylor, K. 1994, *ApJ Lett.*, 422, L9
- Hesser, J. E., Harris, H. C., & Harris, G. L. H. 1986, *ApJ Lett.*, 303, L51
- Huchra, J. P., Brodie, J. P., Kent, S. M., 1991, *ApJ*, 370, 495
- Kravtsov, A., Gnedin, O. 2003 preprint (astro-ph/0305199)
- Larson, R. B., Tinsley, B. M., Caldwell, C. N., 1980, *ApJ*,

- 237, 692
 Li, Y., Mac Low, M., Klessen, R. S., 2004, ApJ, 614, L29
 Minniti, D., Kissler-Patig, M., Goudfrooij, P., Meylan, G.,
 1998, AJ, 115 121
 Mould, J. R., Oke, J. B., de Zeeuw, P. T., & Nemec, J. M.
 1990, AJ, 99, 1823
 Muzzio, J. C., 1987, PASP, 99, 245
 Navarro, J. F., Frenk, C. S., White, S. D. M. 1996, ApJ,
 462, 563
 Peng, E. W., Ford, H. C., & Freeman, K. C. 2004a, ApJ,
 602, 705
 Peng, E. W., Ford, H. C., & Freeman, K. C. 2004b, ApJ,
 602, 685
 Richtler, T. et al., 2004, AJ, 127, 2094
 Searle, L. & Zinn, R. 1978, ApJ, 225, 357
 Sharples, R. 1988, IAU Symp. 126: The Harlow-Shapley
 Symposium on Globular Cluster Systems in
 Galaxies, 126, 545
 Sharples, R. M., Zepf, S. E., Bridges, T. J., Hanes, D. A.,
 Carter, D., Ashman, K. M., & Geisler,
 D. 1998, AJ, 115, 2337
 Shioya, Y., Bekki, K., Couch, Warrick J., De Propris, R.,
 2002, ApJ, 565, 223
 Shioya, Y., Bekki, K., Couch, Warrick J., 2004, ApJ, 601,
 654
 van den Bergh, S., 2000, The Galaxies of the Local Group,
 Cambridge: Cambridge Univ. Press.
 Weil, M. L., Pudritz, R. E., 2001, ApJ, 556, 164
 Weil, M. L., Hernquist, L., 1994, ApJ, 431, L79
 Weil, M. L., Hernquist, L., 1996, ApJ, 460, 101
 Wielen, R., 1977, A&A, 60, 263
 Zepf, S. E., Beasley, M. A., Bridges, T. J., Hanes, D. A.,
 Sharples, R. M., Ashman, K. M., &
 Geisler, D. 2000, AJ, 120, 2928